Time-delay signature concealment of polarization-resolved chaos outputs in vertical-cavity surface-emitting lasers with variable-polarization filtered optical feedback

Li Zhou (周 立), Guangqiong Xia (夏光琼)*, Zhuqiang Zhong (钟祝强), Jiagui Wu (吴加贵), Shuntian Wang (王顺天), and Zhengmao Wu (吴正茂)**

School of Physical Science and Technology, Southwest University, Chongqing 400715, China
**Corresponding author: gqxia@swu.edu.cn; **corresponding author: zmwu@swu.edu.cn*
Received March 13, 2015; accepted June 19, 2015; posted online July 27, 2015

Through employing permutation entropy and the self-correlation function, the time-delay signature (TDS) of a vertical-cavity surface-emitting laser (VCSEL) with variable-polarization filtered optical feedback (VPFOF) is evaluated theoretically. The work shows that the feedback rate η, polarizer angle θ_p, and filter bandwidth Λ have an obvious influence on the TDS. The evolution maps of the TDS in parameter space (η, Λ) and (η, θ_p) are simulated for searching the chaos with weak TDS. Furthermore, compared with a VCSEL with polarization-preserved filtered optical feedback and a VCSEL with variable-polarization mirror optical feedback, this VPFOF–VCSEL shows superiority in TDS suppression.

OCIS codes: 140.1540, 140.7260.
doi: 10.3788/COL201513.091401.

Recently, abundant research has been done to the subject of semiconductor laser (SL)-based or erbium-doped fiber laser (EDFL)-based optical chaos for its various applications such as chaotic radar, secure communication, fast physical random bit generation, optical logic gates[1–8], and so on. Through introducing external perturbations such as optical injection, optoelectronic feedback, or optical feedback[9–12], SLs can be driven into a chaotic output state, where optical feedback SL has been usually regarded as a primary candidate for an optical chaos source since introducing optical feedback can relatively easily yield complex chaos. In general, an obvious time-delay signature (TDS) can be observed in a SL chaotic system with optical feedback[13]. If this TDS-contained chaos signal is used as a carrier in chaos communication, the system security will be threatened since the reconstruction of the SL chaotic system can be realized via some time series analysis methods for chaotic systems[14]. As a consequence, it is indispensable to search for some solutions to conceal the TDS of chaos to ensure the system security. Pre-existing research has proven that through selecting a suitable injection current and feedback strength of the SL, the TDS of chaos in an edge-emitting semiconducting laser (EESL) chaotic system with a single-mirror optical feedback can be suppressed[15]. Simultaneously, through choosing appropriate feedback parameters, the TDS in a double-mirror optical feedback EESL chaotic system can be suppressed[16]. Additionally, after inserting some components with chromatic dispersion such as a fiber Bragg grating (FBG) or a Fabry–Perot-type filter into the optical feedback loop, the TDS of chaos generated by EESLs can also be suppressed[17,18].

As one kind of microchip laser, vertical-cavity surface-emitting lasers (VCSELs) have some superior properties including low threshold current, low cost, single longitudinal mode operation[19,20], and so on. Distinct from EESLs, VCSELs normally emit two polarized components [namely, the x-polarized component (x-PC) and the y-polarized component (y-PC)] because of the weak anisotropies of the material and cavity, which spawns some unique feedback techniques such as polarization-preserved optical feedback (PPOF), polarization-rotated optical feedback (PROF), variable-polarization mirror optical feedback (VPMOF)[21–25], and so on. The TDS suppression of chaos generated by a VCSEL with single-VPMOF or double-VPMOF has been reported[23–25]. Very recently, we used a FBG as the optical feedback device to construct a variable-polarization FBG optical feedback VCSEL (VPFBGOF–VCSEL) chaos system, and then investigated the TDS concealment of chaotic outputs in this system[26]. The result shows that the TDS of the chaos output from the VPFBGOF–VCSEL chaotic system is weaker than that from the VPMOF–VCSEL chaotic system with pure mirror feedback.

In this work, after inserting a filter into the mirror optical feedback loop to supply filtered optical feedback, we propose a chaotic system based on VCSELs under variable-polarization filtered optical feedback (VPFOF) and investigate numerically the TDS of chaos in this chaotic system.

Figure 1 shows a schematic diagram of a VCSEL subject to VPFOF. The output of VCSEL is re-injected into itself after transiting through a beam splitter (BS), a neutral density filter (NDF), a filter, and a polarizer (P).

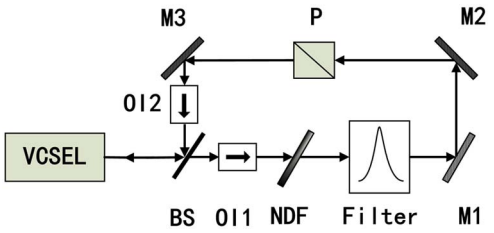

Fig. 1. Schematic diagram of a VESEL subject to VPFOF.

In this system, three mirrors (M1–M3) are used to change the optical path, and two optical isolators (OI1 and OI2) are applied to ensure light unidirectional transmission.

Combining the spin-flip model (SFM)[24–26] with VPFOF[27] for such a chaotic system, the rate equations of a VPFOF–VCSEL can be expressed as

$$\frac{dE_x}{dt} = k(1+i\alpha)(NE_x - E_x + inE_y) - (\gamma_a + i\gamma_p)E_x + \eta F_x(t)\cos^2(\theta_p) + \eta F_y(t)\cos(\theta_p)\sin(\theta_p) + L_x, \tag{1}$$

$$\frac{dE_y}{dt} = k(1+i\alpha)(NE_y - E_y - inE_x) + (\gamma_a + i\gamma_p)E_y + \eta F_y(t)\sin^2(\theta_p) + \eta F_x(t)\cos(\theta_p)\sin(\theta_p) + L_y, \tag{2}$$

$$\frac{dF_{x,y}(t)}{dt} = \Lambda E_{x,y}(t-\tau)e^{-i\omega_0\tau} + (i\Delta\omega - \Lambda)F_{x,y}(t), \tag{3}$$

$$\frac{dN}{dt} = -\gamma_e N(1 + |E_x|^2 + |E_y|^2) + \gamma_e\mu - i\gamma_e n(E_yE_x^* - E_xE_y^*), \tag{4}$$

$$\frac{dn}{dt} = -\gamma_s n - \gamma_e n(|E_x|^2 + |E_y|^2) - i\gamma_e N(E_yE_x^* - E_xE_y^*), \tag{5}$$

where subscript x stands for x-PC and y stands for y-PC, respectively. N indicates the total carrier inversion between the valence band and conduction band, E represents the slowly varied complex amplitude of the field, n is the difference between the carrier inversion of spin-down channel and spin-up radiation channel, α accounts for the line-width enhancement factor, k indicates the decay rate, γ_s is the spin-flip rate, γ_e represents the decay rate for the total carrier, γ_a stands for the linear dispersion, γ_p represents the linear birefringence effect of the active medium, μ indicates the normalized injection current of the chaotic system, τ is the delay time of feedback, and η accounts for the feedback rate. $F(t)$ stands for the slowly varied complex amplitude through the filter, Λ indicates the half-width half-maximum (HWHM) of the filter, ω_0 represents the central angular frequency of the solitary VCSEL, and $\Delta\omega$ is the angular frequency detuning between the filter center frequency and ω_0. The range of polarizer angle θ_p is from 0° to 90°. The equations of spontaneous emission noises are described by the Langevin sources[28]

$$L_x = \sqrt{\frac{\varphi_{sp}}{2}}\left(\sqrt{N+n}\chi_1 + \sqrt{N-n}\chi_2\right), \tag{6}$$

$$L_y = -i\sqrt{\frac{\varphi_{sp}}{2}}\left(\sqrt{N+n}\chi_1 - \sqrt{N-n}\chi_2\right), \tag{7}$$

where χ_1 and χ_2 represent independent Gaussian white noise with unitary variance and zero mean, and φ_{sp} indicates the spontaneous emission rate.

Several approaches can be used to quantitatively evaluate the TDS of chaotic signals, such as the mutual information (MI)[13], self-correlation function (SF)[15], and permutation entropy (PE)[29]. In this Letter, we adopt SF and PE. SF could be described as

$$A(\Delta t) = \frac{\langle[I(t+\Delta t) - \langle I(t)\rangle][I(t) - \langle I(t)\rangle]\rangle}{\sqrt{\langle(I(t+\Delta t) - \langle I(t)\rangle)^2\rangle\langle(I(t) - \langle I(t)\rangle)^2\rangle}}, \tag{8}$$

where $I(t)$ stands for time series of output intensity, $\langle\cdot\rangle$ indicates the time average, and Δt denotes the time shift.

Based on the information principle, PE is proposed and owns some superior advantages such as robustness to noise, fast calculation, and simplicity. PE can be simply described as follows. The intensity time series $\{I(n), n = 1, 2, ..., M\}$ is constructed as a set of C-dimensional vectors through selecting suitable embedded delay time τ_e and dimension C. After that one can study all $C!$ permutation λ of order C. For each λ, the relative probability (ϖ means the number) is defined as

$$p(\lambda) = \frac{\varpi\{n | n \le M - C, (I_{n+1}, ..., I_{n+C}) \text{has types} \lambda\}}{M - C + 1}, \tag{9}$$

and then PE is determined as

$$H(C) = -\sum p(\lambda)\log\, p(\lambda). \tag{10}$$

After considering the suggestions in Ref. [29] and the unique features in VCSELs, the C is set as 7, and then the length of the time series is set as 1.5 us for the calculation of SF and PE.

Equations (1)–(5) can be calculated by a fourth-order Runge–Kutta algorithm. The used parameters are set as follows[30]: $k = 300\ \text{ns}^{-1}$, $\gamma_e = 1\ \text{ns}^{-1}$, $\gamma_p = 10\ \text{ns}^{-1}$, $\gamma_a = 0.1\ \text{ns}^{-1}$, $\gamma_S = 50\ \text{ns}^{-1}$, $\alpha = 3$, $\beta_{sp} = 10^{-6}\ \text{ns}^{-1}$, and $\omega_0 = 2.2176 \times 10^{15}$ rad/s (the corresponding optical wavelength is around 850 nm). The center frequency of the filter is assumed to be identified with that of the VCSEL, i.e., $\Delta\omega = 0$ GHz, and the delay time of the feedback is selected as 3 ns.

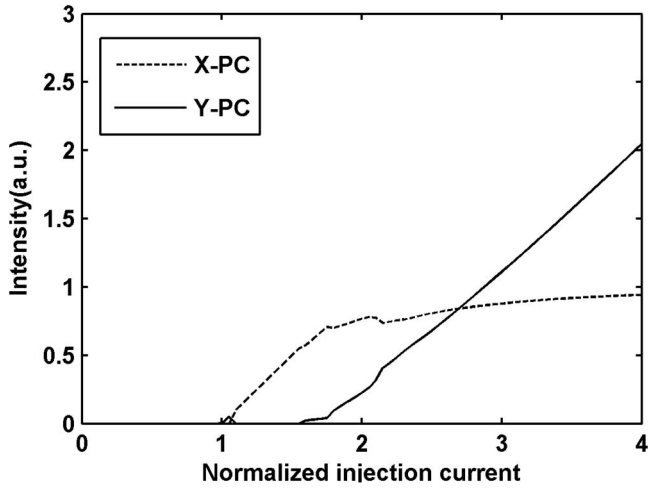

Fig. 2. P-I curve for a solitary running VCSEL, where the dashed line represents the x-PC and the solid line represents the y-PC.

Figure 2 is the P-I curve for a solitary running VCSEL. From Fig. 2, when $\mu = 1$, only the y-PC begins to oscillate. For $1 < \mu < 1.05$, the y-PC continues to oscillate. Once $\mu > 1.05$, the x-PC will oscillate while the y-PC is suppressed. However, when μ exceeds 1.6, the x-PC and y-PC will oscillate together. After taking into account that the simultaneous outputs with similar intensity of the x-PC and y-PC may have potential applications in dual-channel chaos communication or multiple random number generation, in the following we set $\mu = 2.7$ such that the intensity of the x-PC is similar to that of the y-PC.

First, we concentrate on the TDS of the chaos output under fixed Λ and θ_p but different values of η. Figure 3 gives the polarization-resolved time series, power spectra, SF curves, and PE curves of a VPFOF–VCSEL under $\Lambda = 8$ GHz and $\theta_p = 35°$ for different η. As shown in the first row, for $\eta = 0$ ns^{-1}, both the x-PC and y-PC outputs from the VPFOF–VCSEL are periodic states, and the oscillating frequency is about 8.7 GHz. For $\eta = 5$ ns^{-1} (as shown in the second row), from the output time series and the power spectra, one can deduce that the VCSEL enters into a chaotic state. In this case, obvious peaks (or sharp valleys) emerge in the SF (or PE) curves. When η is increased to 15 ns^{-1} (as shown in the third row), the characteristic peaks in the SF and PE curves are suppressed efficiently. However, further increasing η to 28 ns^{-1} (as shown in the fourth row), the TDS arises again.

Second, we investigate the influence of the polarizer angle θ_p on the TDS. Figure 4 gives the corresponding results for $\theta_p = 0°$ [Fig. 4(a)], $\theta_p = 30°$ [Fig. 4(b)], $\theta_p = 60°$ [Fig. 4(c)], and $\theta_p = 90°$ [Fig. 4(d)], where Λ and η are fixed at 8 GHz and 15 ns^{-1}, respectively. It should be noted that the case of $\theta_p = 0°$ and $\theta_p = 90°$ correspond to a pure x-PC optical feedback and a pure y-PC optical feedback, respectively. From Fig. 4, it can be seen that, for $\theta_p = 30°$, the TDS of both the x-PC and y-PC can be suppressed simultaneously. For a relatively small value of θ_p, the TDS of the x-PC is more obvious than that of the y-PC. However, for a relatively large value of θ_p, the opposite conclusion is obtained. Especially, when θ_p is taken as 90°, the intensity of the x-PC is suppressed [Fig. 4(d)]. The simulated results show that an intermediate polarizer angle is helpful to make the x-PC and y-PC possess similar TDS and output intensity.

Next, we research the total evolution of the TDS of the polarization-resolved output from the VPFOF–VCSEL in the parameter space of η and Λ. Here, the amplitude σ, defined as the maximum of the SF peak at the Δt range of [2.7 ns, 3.3 ns], is selected to distinguish the obvious degree of TDS. A small value of σ indicates a weak TDS. If $\sigma < 0.1$, the TDS can be regarded to be well-suppressed. Figure 5 shows the maps of σ under different η and Λ for a VCSEL subject to VPFOF with $\theta_p = 10°$ [Fig. 5(a)], $\theta_p = 40°$ [Fig. 5(b)], $\theta_p = 70°$ [Fig. 5(c)], and polarization-preserved filtered optical feedback (PPFOF) [Fig. 5(d)]. Within Fig. 5, the regions surrounded by the dashed lines are for $\sigma < 0.1$, and the white region corresponds to the case that one of polarized components has been suppressed and its intensity is much smaller than the other polarized component. From these maps of TDS (i.e., Fig. 5), one

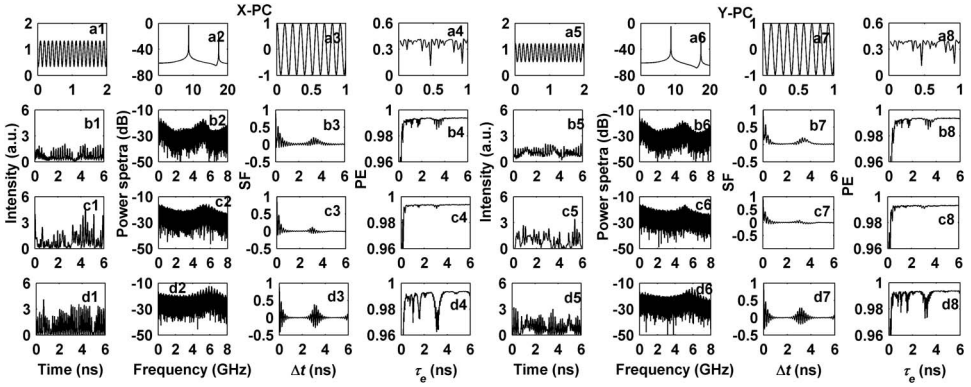

Fig. 3. Polarization-resolved time series (first and fifth columns), power spectra (second and sixth columns), SF curves (third and seventh columns), and PE curves (fourth and eighth columns) of a VPFOF–VCSEL under $\Lambda = 8$ GHz and $\theta_p = 35°$ for $\eta = 0$ ns^{-1} (first row), $\eta = 5$ ns^{-1} (second row), $\eta = 15$ ns^{-1} (third row), and $\eta = 28$ ns^{-1} (fourth row).

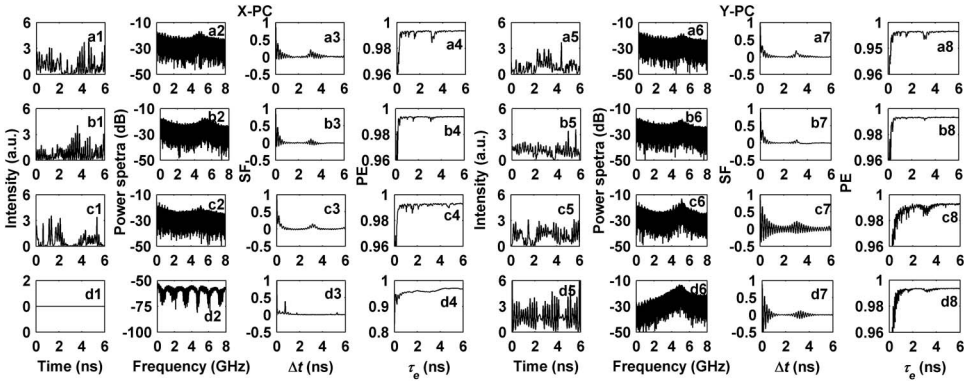

Fig. 4. Polarization-resolved time series (first and fifth columns), power spectra (second and sixth columns), SF curves (third and seventh columns), and PE curves (fourth and eighth columns) of a VPFOF–VCSEL under $\Lambda = 8$ GHz and $\eta = 15$ ns^{-1} for $\theta_p = 0°$ (first row), $\theta_p = 30°$ (second row), $\theta_p = 60°$ (third row), and $\theta_p = 90°$ (fourth row).

could observe that, for $\theta_p = 10°$, the parameter space for generating two TDS completely suppressed PCs ($\sigma < 0.1$) is relatively large. For $\theta_p = 40°$, the region within which the TDS of PCs is completely suppressed is shifted and slightly decreased compared with that for $\theta_p = 10°$. However, for $\theta_p = 70°$, the region with completely suppressed

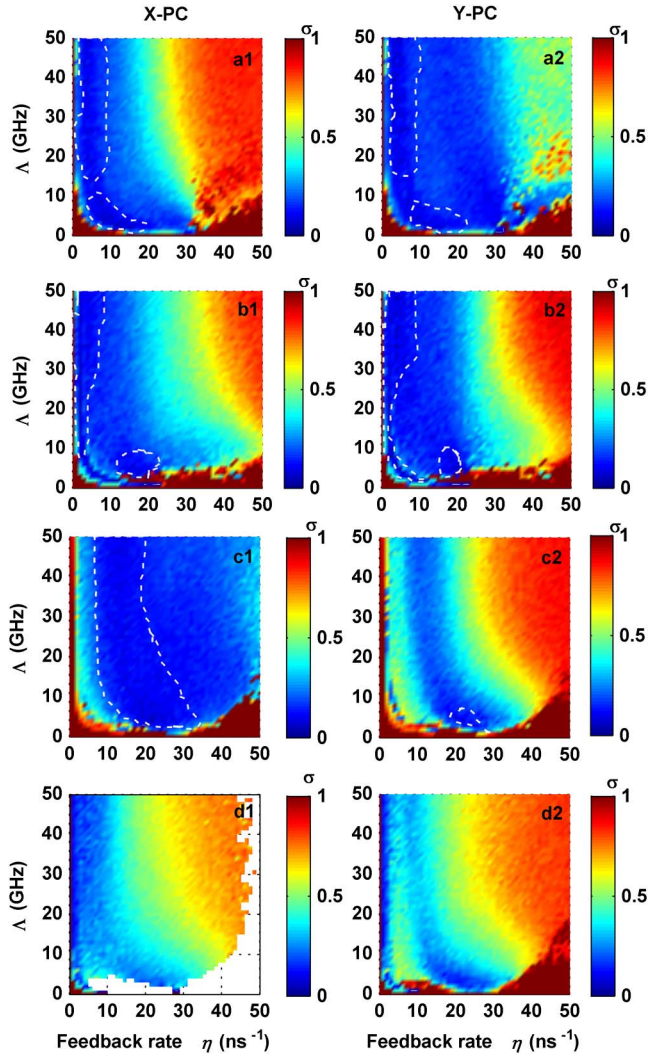

Fig. 5. Maps of σ under different η and Λ for a VCSEL subject to VPFOF with (a) $\theta_p = 10°$, (b) $\theta_p = 40°$, (c) $\theta_p = 70°$, and (d) PPFOF.

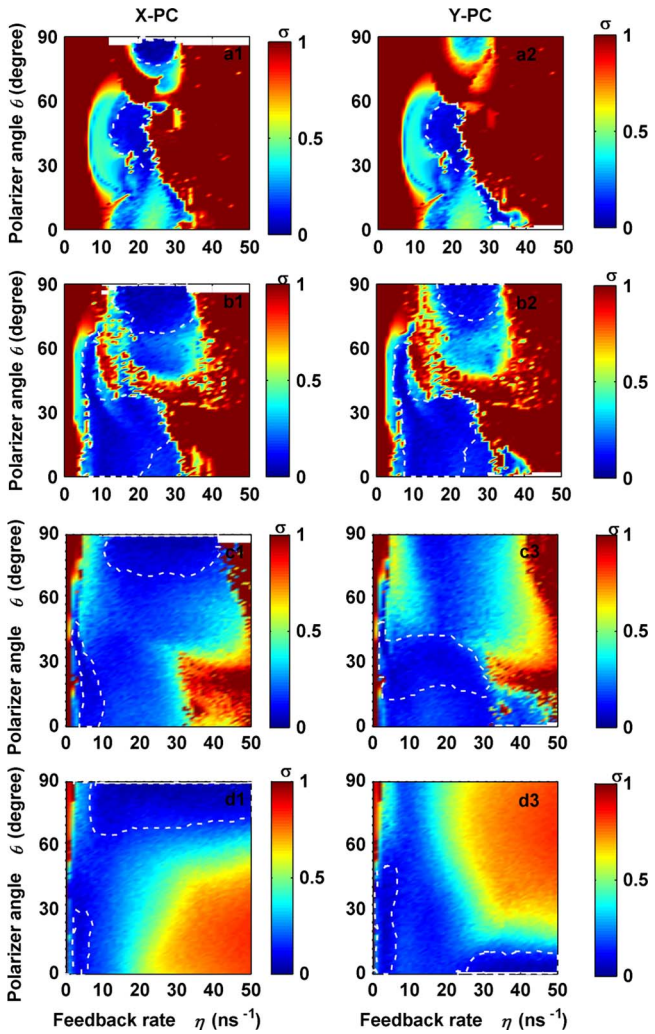

Fig. 6. Maps of σ under different η and θ_p for a VCSEL subject to VPFOF with (a) $\Lambda = 1$ GHz, (b) $\Lambda = 3$ GHz, (c) $\Lambda = 8$ GHz, and (d) VPMOF.

TDS is very broad for the x-PC but very narrow for the y-PC. The aforementioned results show that θ_p seriously affects the parameter space region for generating two PCs with completely suppressed TDS. Additionally, it can also be observed that under the aformentioned three θ_p, VPFOF is superior to PPFOF for achieving polarization-resolved chaotic outputs with weak TDS.

Finally, we give the maps of σ under different η and θ_p for VCSELs subject to VPFOF with $\Lambda = 1$ GHz [Fig. 6(a)], $\Lambda = 3$ GHz [Fig. 6(b)], $\Lambda = 8$ GHz [Fig. 6(c)], and VPMOF [Fig. 6(d)]. Figure 6 indicates that with increasing Λ, the regions of simultaneously suppressed TDS for the x-PC and y-PC move towards the relatively small feedback rates, which can be explained by the fact that the x-PC and y-PC locate closely at the center peak of the filter and possess larger transmittance in the case of larger Λ. As a result, a smaller η is inquired for achieving a similarly effective feedback rate under a larger Λ. Furthermore, through carefully observing Fig. 6, it can be seen that compared with the case of VPMOF–VCSEL, under an optimized value of Λ 3 GHz), the VPFOF–VCSEL has a broader region where the TDS of the x-PC and y-PC can be well-suppressed simultaneously ($\sigma < 0.1$).

In conclusion, we research and numerically analyze the TDS in a chaotic system based on a VCSEL subject to VPFOF. By using the analytic techniques of SF and PE, the TDS of the chaos output can be quantitatively evaluated, and then the effects of feedback rate, polarizer angle, and filter bandwidth of the filter on the TDS of the chaotic outputs are analyzed. The results show that, through optimizing some operation parameters, the TDS of polarization-resolved outputs from the VPFOF–VCSEL can be simultaneously suppressed. In comparison with a PPFOF (or VPMOF) VCSELs chaos system, such a VPFOF–VCSEL system shows some superiority in simultaneously acquiring polarization-resolved chaotic signals with weak TDS.

This work was supported by the National Natural Science Foundation of China (Grant Nos. 61178011, 61275116, and 61475127) and the Graduate Research and Innovation Project of Chongqing Municipality (Grant No. CYB14054).

References

1. A. Argyris, D. Syvridis, L. Larger, V. A. Lodi, P. Colet, I. Fischer, J. G. Ojalvo, C. R. Mirasso, L. Pesquera, and K. A. Shore, Nature **438**, 343 (2005).
2. S. Yan, Chin. Opt. Lett. **3**, 283 (2005).
3. X. Dou, C. Wu, X. Chen, H. Yin, Q. Zhao, Y. Hao, and N. Zhao, Chin. Opt. Lett. **12**, S10610 (2014).
4. H. P. Hu, X. F. Chen, W. Su, F. L. Xie, and X. J. Gao, Acta Opt. Sin. **34**, 0406006 (2014).
5. Y. J. Liu, S. H. Zhang, H. Yang, and J. F. Tan, Chin. J. Lasers **39**, 0905004 (2012).
6. F. Y. Lin and J. M. Liu, IEEE J. Quantum Electron. **40**, 682 (2004).
7. A. Uchida, K. Amano, M. Inoue, K. Hirano, S. Naito, H. Someya, I. Oowada, T. Kurashige, M. Shiki, S. Yoshimori, K. Yoshimura, and P. Davis, Nat. Photon. **2**, 728 (2008).
8. M. Ma, Z. Hu, P. Xu, W. Wang, and Y. Hu, Chin. Opt. Lett. **12**, 081403 (2014).
9. J. Mork, B. Tromborg, and J. Mark, IEEE J. Quantum Electron. **28**, 93 (1992).
10. T. B. Simpson, J. M. Liu, A. Gavrielides, V. Kovanis, and P. M. Alsing, Phys. Rev. A **51**, 4181 (1995).
11. Y. Guo, Y. Wu, and Y. Wang, Chin. Opt. Lett. **10**, 061901 (2012).
12. Y. Y. Xie, Z. M. Wu, T. Deng, X. Tang, L. Fan, and G. Q. Xia, IEEE Photon. Technol. Lett. **25**, 1605 (2013).
13. J. G. Wu, G. Q. Xia, X. Tang, X. D. Lin, T. Deng, L. Fan, and Z. M. Wu, Opt. Express **18**, 6661 (2010).
14. V. S. Udaltsov, J. P. Goedgebuer, L. Larger, J. B. Cuenot, P. Levy, and W. T. Rhodes, Phys. Lett. A **308**, 54 (2003).
15. J. G. Wu, G. Q. Xia, L. P. Cao, and Z. M. Wu, Opt. Commun. **282**, 3153 (2009).
16. J. G. Wu, G. Q. Xia, and Z. M. Wu, Opt. Express **17**, 20124 (2009).
17. S. S. Li, Q. Liu, and S. C. Chan, IEEE Photon. J. **4**, 1930 (2012).
18. Y. Wu, B. J. Wang, J. Z. Zhang, A. B. Wang, and Y. C. Wang, Math. Probl. Eng. **2013**, 571393 (2013).
19. F. Koyama, J. Lightwave Technol. **24**, 4502 (2006).
20. M. Virte, K. Panajotov, H. Thienpont, and M. Sciamanna, Nat. Photon. **7**, 60 (2013).
21. R. Ju, P. S. Spencer, and K. A. Shore, IEEE J. Quantum Electron. **41**, 1461 (2005).
22. H. Lin, Y. H. Hong, and K. A. Shore, J. Lightwave Technol. **32**, 1829 (2014).
23. S. Priyadarshi, Y. H. Hong, I. Pierce, and K. A. Shore, IEEE J. Sel. Top. Quantum Electron. **19**, 1700707 (2013).
24. S. Y. Xiang, W. Pan, B. Luo, L. S. Yan, X. H. Zou, N. Jiang, L. Yang, and H. N. Zhu, Opt. Commun. **284**, 5758 (2011).
25. P. Xiao, Z. M. Wu, J. G. Wu, L. Jiang, T. Deng, X. Tang, L. Fan, and G. Q. Xia, Opt. Commun. **286**, 339 (2013).
26. Y. Li, Z. M. Wu, Z. Q. Zhong, X. J. Yang, S. Mao, and G. Q. Xia, Opt. Express **22**, 19610 (2014).
27. A. P. A. Fischer, M. Yousefi, D. Lenstra, M. W. Carter, and G. Vemuri, IEEE J. Sel. Top. Quantum Electron. **10**, 944 (2004).
28. S. Y. Xiang, W. Pan, B. Luo, L. S. Yan, X. H. Zou, N. Jiang, N. Q. Yang, and H. N. Zhu, IEEE Photon. Technol. Lett. **24**, 1267 (2012).
29. C. Bandt and B. Pompe, Phys. Rev. Lett. **88**, 174102 (2002).
30. I. Gatare, M. Sciamanna, A. Locquet, and K. Panajotov, Opt. Lett. **32**, 1629 (2007).